CONFERENCE PRE-PRINT

VERIFICATION AND OPTIMIZATION OF THE VDE BY COUPLING THE FREE-BOUNDARY EQUILIBRIUM AND FAST TRANSPORT CODES WITH CONTROL IN THE HL-3 TOKAMAK

EX-S

X. SONG, L. XUE, Y-H. CHENG, J-Z. ZHANG, T-F. SUN, Y-H. ZHANG, Y-Y. ZHONG, D. LI, P-L. LIU, L. LIU, J-X LI, S. WANG, H-L. DU, M. XUE, G-Y. ZHENG, W-L. ZHONG Southwestern Institute of Physics, Chengdu, 610041, China

Email: songx@swip.ac.cn

Abstract

An integrated workflow has been developed to verify and optimize the VDE predictions in the HL-3 tokamak. The workflow is divided into two parts, i.e. plasma control and the non-linear plasma model. The plasma model is designed to represent the evolution of core parameters and profiles, while the plasma control loop remains the same as the one embedded in the PCS. The objectives of feedback (FB) control are R, Z and I_p , with the control strategy based on coil voltages. The reference trajectories for the control objectives and coil voltages in feedforward (FF) settings are determined through optimization or trial and error by pilots. The non-linear plasma model, which is numerically coupled using the free-boundary equilibrium code FEEQS.M, the fast transport code METIS and a simplified evolution of plasma current. The integrated workflow is first used to verify #3293 with a VDE event in the HL-3. The results of prediction by the integrated modeling, in terms of coil currents and voltages, R, Z, I_p , κ , δ , β_p and l_i , are almost overlapping with experimental observations. With the aforementioned verification, the workflow is then applied to optimize the nominal shot to avoid VDE-induced disruption. It is found that, using the experimental controller gains with optimization for R^{Ref} , the dynamic scenario remains a smooth shape transition with oscillations in toroidal current diffusion as experiment. In the future, improved transport models and surrogate neural network approaches will be deployed to analyze more complicated pulses with auxiliary heating powers and run simulations in a fast manner.

1. INTRODUCTION

Tokamak is one of the promising paths toward achieving a clean and environmentally friendly power source, by utilizing nuclear fusion in a peaceful way, for the grid in the coming decades [1]. For a tokamak reactor, it's essential to simultaneously maintain a nominal plasma current (I_p) and a specific plasma shape, like the X-point configuration. This precisely requires a particular magnetic field, characterized by toroidal (B_ϕ) and poloidal (B_p) components, induced by external coil currents and plasma current through a sophisticated way. The specific magnetic field configuration is crucial to ensure compatibility with high confinement and to facilitate the exhaust of particles and power from the plasma boundary to the plasma facing components (PFCs) or first wall. Failure to synchronize the control of the magnetic field in a tokamak reactor can have serious consequences. It not only prevents the plasma from reaching the desired burning state but also increases the risk of off-normal events, such as major disruptions. These events could pose safety challenges to large-scale machines like ITER and future FPP (fusion pilot plant), which are designed for burning plasmas with high energy neutrons.

Vertical displacement events (VDEs) [2] are one of the main causes of major disruption that could damage PFCs, especially in reactor-size tokamaks. For example, only two major disruptions are allowed throughout all stages of ITER operation. Elongated plasma, an effective approach to enable high plasma confinement, is inherently vertically unstable. Additionally, perturbations in other parameters, such as poloidal beta β_p , internal inductance l_i and toroidal current density j_{ϕ} , can also increase the vertical growth rate of VDEs, making it very difficult to reliably control the plasma vertical position. Therefore, it is a high priority to evaluate VDEs in closed-loop simulation with high-fidelity models.

Reliable integrated simulations of control-oriented plasma models are among the top priorities for studying and evaluating behaves of VDE within the tokamak community. These controls are dominantly categorized into two types, i.e. magnetic control and kinetic control. Magnetic control mainly focuses on the plasma current and plasma shape, from ramp-up (right after the formation of closed magnetic surface) to flat-top and finally to plasma ramp-down phases, where the model is based on the Grad-Shafranov (G-S) equilibrium equation [3]. Whereas the objective of magnetic control is to maintain the specified plasma shape, e.g., so called X-divertor [4] and snowflake configurations, to reduce wall recycling on impurities and power exhaust,

and the objective of kinetic control is to reduce transport and produce edge and internal transport barriers in plasma profiles such as electron temperature (T_e) , where an internal electron transport barrier (e-ITB) is found on recent EAST campaign to enable one thousand seconds "super" improved mode (I-mode) operation [5]. The calculation of the q-profile relies on the Magnetic Diffusion Equation (MDE) as detailed in [6], while the evolution of electron temperature is determined by the Electron Heat Transport Equation (EHTE) as explained in [7]. Predictive integrated modeling involves the integration of equilibrium, MDE, and transport solvers, along with their associated sources and sinks. This integration enables simulations for the simultaneous application of magnetic and kinetic controls, a task known for its inherent complexity. The complexity of this task primarily arises from dealing with different dimensional aspects. For instance, the free-boundary equilibrium (FBE) involves a 2D problem in (R, Z) coordinates, which requires iterative solutions due to the non-linearity of the toroidal plasma current density in the G-S equation. On the other hand, the MDE and transport equations are 1D problems, based on the normalized toroidal flux radius, and they involve non-linear heating and non-inductive current sources from other complex methods. This is why some current model-based control-oriented simulations tend to focus either on magnetic control with simplified transport coefficient profiles, or on kinetic control with simplified equilibrium parameters. Importantly, these integrated simulations rely heavily on intensive calculations performed by integrated modeling codes like TRANSP [8], ASTRA [9], CORSICA [10], JINTRAC [11], and DINA [12]. However, this heavy computational burden often hinders the ability to conduct fast controloriented scenario designs and developments.

In this work, a fast coupling architecture is developed to integrate the FBE and fast transport (FT) solvers, including MDE. The basic idea is similar to a recent work for NSTX-U [13], where the evolution of plasma boundary is calculated with TRANSP predicted j_{ϕ} . This architecture is designed for model-based, control-oriented simulations focused on the HL-3 tokamak. The coupling process involves the exchange of profiles and parameters between the equilibrium and transport solvers. A self-consistent plasma current model is developed based on parameters from FBE and FT calculations. The transport equations have been efficiently solved using METIS [14] library of models, which encompass various complexities designed to suit different control applications. These models include analytical, scaling laws, empirical, and neural network models trained from physics-based codes. In addition to the FBE and FT models, The objective of FF and FB strategy as well as the gains in the PID controller are also aligned with the "real" PCS. Finally, the integrated scheme is applied to study the HL-3 scenario with VDE-reduced disruption from ramp-up phase, demonstrating self-consistent results between the closed-loop simulations and experimental observations. The organization of this paper is as follows: Section 2 presents the equilibrium, transport equations, plasma current mode and their couplings in an evolutive way. The dedicated simulation and optimization of VDE-induced pulse for the HL-3 is detailed in Section 3. In Section 4, the conclusion is provided, and potential future work is outlined.

2. A NOVEL INTEGRATED WORKFLOW WITH CONTROL STRATEGY

An integrated workflow, based on the evolution of FBE and transport equations and I_p model, is developed to verify and optimize the VDE predictions in the HL-3 tokamak. In addition, a specified control strategy is used to regulate the plasma quantities in a desired direction. In this section, all the equations and models are detailed.

2.1. G-S Equilibrium Equation and Its Time Evolution

Due to the toroidally axisymmetric assumption in tokamak geometry, only the cylindrical coordinate system consisting of (R, Z) is taken into account. The G-S equation for the FBE problem, which is derived from the force balance equation, is expressed as stated in [15]

$$\Delta^* \psi(R, Z) = -\mu_0 R J_\phi(R, Z), \tag{1a}$$

$$\Delta^* \equiv R \frac{\partial}{\partial R} \left(\frac{1}{R} \frac{\partial}{\partial R} \right) + \frac{\partial^2}{\partial Z^2}. \tag{1b}$$

The poloidal flux function ψ , which represents the poloidal magnetic flux per radian, is defined as $\psi(R,Z) \equiv RA_{\phi}$ based on the equation $B = \nabla \times A$ (with $\nabla \cdot B = 0$). Here, μ_0 represents the permeability in a vacuum region. The toroidal plasma current density $J_{\phi}\big(R,\psi(R,Z),t\big)$ in (1a) with respect to time represents the toroidal current density and varies depending on different regions

$$J_{\phi}\big(R,\psi(R,Z,t),t\big) = \begin{cases} Rp'\big(\psi(R,Z,t)\big) + \frac{ff'\big(\psi(R,Z,t)\big)}{\mu_0 R} & \text{in plasma area } \Omega_{pl}\big(\psi(R,Z,t)\big) \\ \frac{I_i}{S_i} & \text{in coil number } 1 \leq i \leq M \\ j_S = -\frac{\sigma}{R} \frac{\partial \psi(t)}{\partial t} & \text{in S (passive plates)} \\ 0 & \text{elsewhere} \end{cases}$$
(2)
$$\frac{I_i}{S_i} = \sum_{j=1}^N R_{ij} V_j(t) + \sum_{k=1}^M C_{ik} \int_{C_k} \frac{\partial \psi(t)}{\partial t} \, dR dZ \,, \, 1 \leq i \leq M, \, R_{ij} = \begin{cases} 0 & i \neq j \\ \frac{n_i}{R_i S_i} & i = j \end{cases} C_{ij} = \begin{cases} 0 \\ -\frac{2\pi n_i^2}{R_i S_i^2}. \end{cases}$$

Here p represents plasma kinetic pressure, σ is the conductivity of passive plates, f is the diamagnetic function defined as $f(\psi) \equiv RB_{\phi}$, and I_i , R_{ii} , n_i and S_i denote the current, resistance, total number of turns and cross-section of external conductor coil i, respectively. Both p and f are functions dependent on ψ . It is beneficial to introduce the normalized poloidal flux function, denoted as $\psi_N = (\psi - \psi_{ax})/(\psi_{bd} - \psi_{ax})$, ensuring it ranges from 0 at the magnetic axis (ψ_{ax}) to 1 at the plasma boundary (ψ_{bd}) . To expedite the execution of the FBE solver, we use the equilibrium results from previous runs, including coil currents and the ψ map, as the initial guess for the next FBE calculation.

In this work, only the direct evolution of FEEQS.M [16] is employed. Input for the direct evolution mode of FEEQS.M includes coil voltages, $J_{\phi}(R, \psi(R, Z), t)$ which is read from METIS and total I_p , while outputs are the $\psi(R, Z, t)$ associated with coil currents.

2.2. Transport Equations

Unlike the FBE in FEEQS.M, which is determined on the (R, Z) coordinates, the transport equations are performed using the effective minor radius, ρ , with the toroidal flux, Φ .

$$\Phi \equiv \pi B_0 \rho^2 \ , \ \rho_b \equiv \sqrt{\frac{\Phi_b}{\pi B_0}} \ , \ \hat{\rho} \equiv \frac{\rho}{\rho_b} \in [0, 1], \tag{3}$$

where, Φ_b represents Φ at the plasma boundary, B_0 is the toroidal magnetic field at the major radius R_0 , $\hat{\rho}$ is the normalized effective minor radius, and ρ_b is the effective minor radius at the plasma boundary.

The MDE and its boundary conditions are defined as follows

$$\frac{\partial \psi}{\partial t} = \frac{\eta(T_e)}{\mu_0 \rho_b^2 F^2} \frac{1}{\hat{\rho}} \frac{\partial}{\partial \hat{\rho}} \left(\hat{\rho} F G H \frac{\partial \psi}{\partial \hat{\rho}} \right) + \frac{R_0 H \eta(T_e)}{B_0} \langle j_{\text{NI}} \cdot B \rangle \tag{4a}$$

$$\mathbf{B.C.} : \frac{\partial \psi}{\partial \hat{\rho}} \Big|_{\hat{\rho}=0} = 0; \ \frac{\partial \psi}{\partial \hat{\rho}} \Big|_{\hat{\rho}=1}^{t} = -\frac{\mu_0 R_0}{2\pi G H} I_p(t). \tag{4b}$$

Here, $\eta(T_e)$ represents plasma resistivity, which is dependent on the electron temperature T_e , $j_{\rm NI}$ stands for non-inductive plasma current, encompassing contributions from bootstrap and auxiliary current drive methods such as E/ICCD, LHCD, and NBCD. The flux-averaged $<\cdot>$ quantities F, G, and H are equilibrium parameters that defined as follow

$$F = \frac{R_0 B_0}{f} , G = \langle \frac{R_0^2 |\nabla \rho|^2}{R^2} \rangle , H = \frac{F}{\langle R_0^2 / R^2 \rangle}$$
 (5)

Additionally, the electron density profile (n_e) is determined by the line-averaged electron density (\overline{n}_e) .

$$n_e(\hat{\rho}, t) = n_e^{prof} \overline{n}_e(t), \tag{6}$$

where n_e^{prof} is typically read from experiment. In this work, only scaling laws for the evolution of T_e and $j_{\rm NI}$ are considered.

The inputs for METIS are I_p , \overline{n}_e , $Z_{\rm eff}$, heating powers (not included in this work), plasma equilibrium parameters, i.e, $R_0, Z_0, a, \kappa, \delta$, from FEEQS.M, respectively. Whereas the output for FEEQS.M is $J_\phi(R, \psi(R, Z), t)$. The transport equation solvers in METIS utilize finite difference method within the Matlab/Simulink environment, a widely adopted platform for control design across development stages. METIS provides an extensive library of models with varying complexities to suit diverse control applications, including analytical models, scaling laws, empirical models, and neural-network models trained from physics-based codes [17].

2.3. Plasma Current Model

As discussed above, both FEEQS.M and METIS start with a given I_p . It is therefore necessary to construct a time evolution of plasma current that is consistent with the parameters obtained from the equilibrium and fast transport solvers by

$$V_{loop} = R_p(I_p - I_p^{NI}) + L_p \frac{dI_p}{dt}$$

$$V_{loop} = -2\pi \frac{\partial \psi_{bnd}^{FEEQS.M}}{\partial t}, \quad L_p = \mu_0 R_0 \left(\ln(8 \frac{R_0}{a} \sqrt{\frac{2}{1 + \kappa^2}}) - 2 + \frac{l_i}{2} \right)$$
(7)

where R_p and $I_p^{\rm NI}$, represents the plasma resistance (Spitzer or Sauter [18] model w.r.t Te) and non-inductive plasma current (in this work, only bootstrap and runway components are considered) provided by METIS. The other parameters such as, loop voltage (V_{loop}), self inductance (L_p) in terms of minor radius (a), elongation (κ), triangulation (δ) and internal inductance (l_i), are given by FEEQS.M.

With this plasma current evolution, the equilibrium and fast transport models can run in a self-consistent way to determine all the other core plasma quantities.

2.4. Integrated Model with Feedback Control Strategy

The integrated model for the evolution of plasma parameters consists of three parts, i.e. the evolution of FBE, MDE and I_p model. To compare simulation results with experimental data, a feedback (FB) control strategy is required to enable a closed-loop plasma simulation with desired target parameters. The control strategy is the same as that applied in the "real" PCS of HL-3. The FB control targets are R, Z and I_p , with coil voltages (V_{PF}) serving as the control actuators. It should be noted that coil currents are not explicitly involved in the FB loop. The reference trajectories for R, Z, I_p and V_{PF} in FF settings are determined either through model-based optimization or pilot-guided trial and error. The gains of the PID controller are also aligned with those used in the PCS. The total output of V_{PF} combined with FF and FB is computed as

$$\begin{split} V_{PF}^{Total} &= V_{PF}^{FF} + V_{PF}^{FB} \\ V_{PF}^{FB} &= V_{PF,R}^{FB} + V_{PF,Z}^{FB} + V_{PF,I_p}^{FB} \\ V_{PF,R}^{FB} &= \Delta R * \text{PID} * M_{matrix,R} \;, \; \textit{Same methods w.r.t Z and } I_p, \end{split} \tag{8}$$

where ΔR (w.r.t $\Delta Z, \Delta I_p$) is the deviation of radial position in simulation from reference, PID is the gain parameter, and $M_{matrix,R}$ [19] is the control matrix based on desired plasma shape.

Finally, the coupled workflow based on the integrated plasma models and control strategy can be used to validate the HL-3 experiments. Fig. 1 presents the schematic of integrated workflow, where black dashed lines represent for on-line plasma operations.

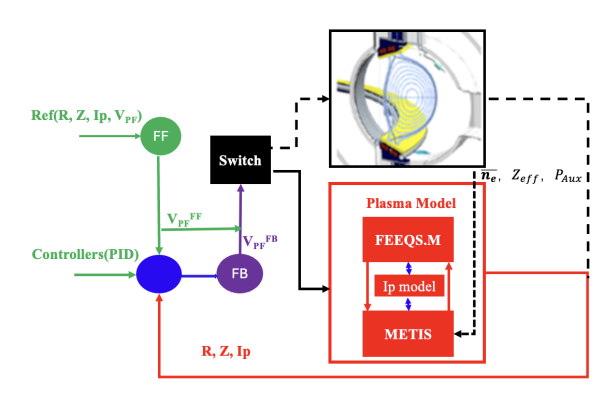


FIG. 1. Schematic of the integrated workflow.

3. VERIFICATION AND OPTIMIZATION OF THE VDE BY THE INTEGRATED WORKFLOW FOR A NOMINAL HL-3 PULSE

The developed workfolw is deployed to virtually replay a dedicated shot, i.e. #3293, which terminates with a VDE induced disruption during I_p ramp-up phase. The objective of #3293 is to achieve a nominal diverted plasma shape with $I_p \sim 1.5$ MA, $\kappa \sim 1.5$ and $\delta \sim 0.5$. However, due to the limited flux swing capacity provided by CS and PF coils to sustain such a high I_p , the plasma shape must quickly transition from limiter to divertor configuration to reduce Ohmic consumption. This requires κ to increase from 1.0 to 1.5 during the ramp-up phase. Such a dynamic scenario introduces significant oscillations, e.g., j_{ϕ} evolves drastically in response to variations in β_p and l_i . These rapid changes are accompanied by fast modifications in R, R and R are the only available actuators. Ultimately, this highly dynamic shot terminates with a VDE-induced disruption.

The coupled workflow is first applied to replay the nominal shot with the same control strategy, i.e. FF and FB, consistent with their applications in PCS. By analyzing the simulation results, an optimization with modified FF settings, in terms of a new reference trajectory, is then deployed to reliably avoid the VDE during the continued increase of I_p .

3.1. Verification of VDE by Simulation

To replay #3293 with the same settings from the PCS, the initial equilibrium and j_{ϕ} must be aligned with the experimental conditions, i.e. the plasma boundary and coil currents provided by EFIT [20] and measurements, respectively. The initial equilibrium calculated by FEEQS.M, in which β_p and l_i are estimated from METIS, is constrained to match the EFIT boundary and coil currents (including eddy currents on vacuum vessel) by adjusting PF8U/L currents by -0.2 and 0.1 kA/turn,

respectively. It should be noted that in the coupled workflow I_p is calculated using Eq. 7, while R and Z are computed through an E-Matrix [21], as applied in PCS. The verification starts from $t_0 = 140 \, ms$, when the FB strategy in PCS is activated.

The verification results are shown in Fig. 2. It is evident that the plasma boundary and geometry parameters, κ and δ presented in (e.), follow the EFIT results well from the limiter to divertor phase before the VDE-induced disruption occurs at about $600 \, ms$, where the X-points are nearly overlapped. The trajectories of R and I_p also agree closely with the experimental results and follow the reference values. However, Z matches well while the plasma shape remains in the limiter phase (before 300ms), but deviates after transitioning to the divertor configuration, responding more rapidly than in the experiment during the VDE disruption. The eddy current (I_{vv}) , shown in (f.), deviates in the limiter phase but agrees better in the divertor phase, indicating that the R_p and vacuum vessel are effectively modeled during the divertor regime. The overlapping β_p and I_i , given in (d.), between FEEQS.M and METIS further demonstrates consistency between the equilibrium and transport simulations.

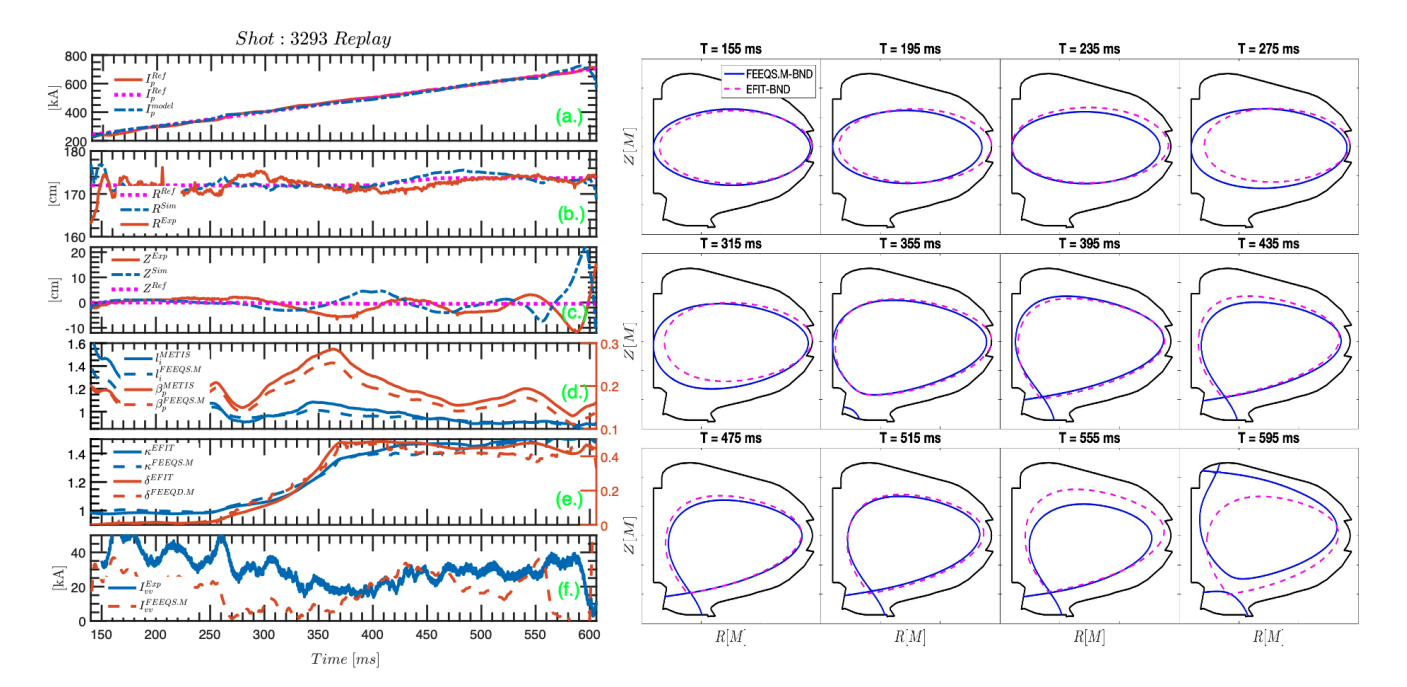


FIG. 2. Left: comparison between simulation and experiment for #3293, (a) I_p , (b) R, (c) Z, (d) β_p and l_i , (e) κ and δ , (f) I_{vv} . Right: plasma boundary between magnetics-constrained EFIT and FEEQS.M.

The evolution of coil currents and voltages, together with their comparison to experiments, are shown in Figs. 3 and 4. The dominant coil for controlling I_p are CS, PF6 and PF8, for controlling R are PF1 and PF8, and for controlling Z are PF2, PF3, PF6 and PF7. In general, I_{PFs} obtained from FEEQS.M simulations agree well with experimental values. The higher I_{CS} observed between 300ms to 400ms indicates that R_p is underestimated by METIS during the plasma transition from limiter to divertor. The good agreement of $I_{PF1,8}$ suggests R is consistent between simulation and experiment. The deviations in $I_{PF6,7}$ are aligned with the previously discussed difference in Z. The well-tracked coil voltages further confirm that the circuit equations embedded in FEEQS.M are valid.

3.2. Analysis of VDE Disruption through Simulation

With the aforementioned verification, the coupled workflow is subsequently applied to analyze the causes of the VDE-induced disruption in #3293. A straightforward approach is to examine the estimation of R, Z, which in the experiment are calculated in real time by multiplying diagnostic magentics and coil currents with a given E-Matrix. The components of E-matrix include coil currents (CS, PF, TF) and magnetics (flux and field).

The comparison of R,Z from experiments (E-Matrix) and from FEEQS.M (current barycenter) is presented in Fig. 5. It is obviously found that R-EMartix is smaller than R_{Bary} -FEEQS.M, whereas Z-EMartix is similar to Z_{Bary} -FEEQS.M, except that Z_{Bary} -FEEQS.M responds more fast than Z-EMartix. A noticeable bump appears in R-EMartix between 250ms and 350ms, during plasma shape transition from limiter to divertor. A possible explanation for this bump is the modification of j_{ϕ} , i.e. the oscillation in β_p shown in (d.) of Fig. 2. Variations in j_{ϕ} alter the magnetic field in magnetics, which in turn affect the estimation of R,Z. It should be noted that the exact causes, e.g., modification of plasma internal profiles and potential microor macro-MHD instabilities, leading to the VDE-induced disruption are complex and difficult to identify conclusively.

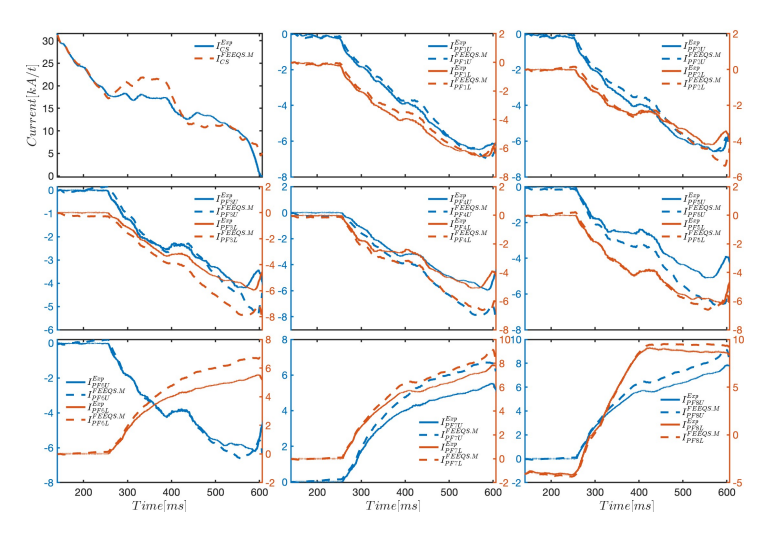


FIG. 3. Comparison of I_{PFs} between FEEQS.M simulation (dashed line) and experiment (plain line) for #3293.

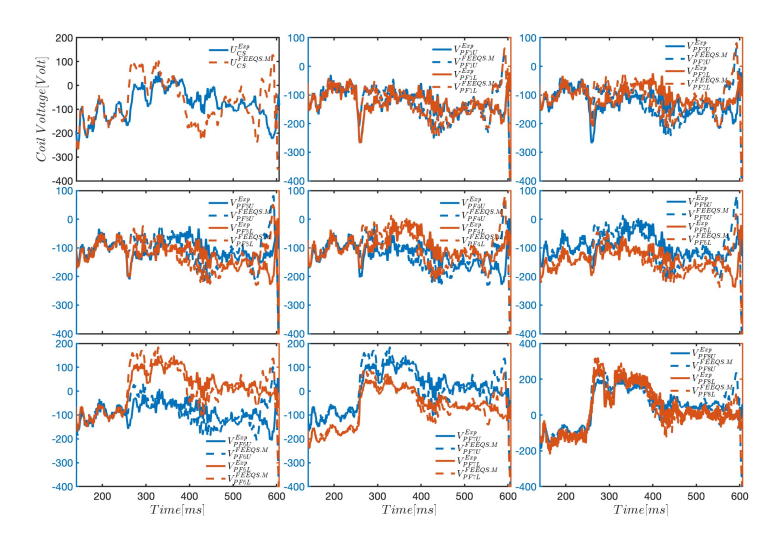
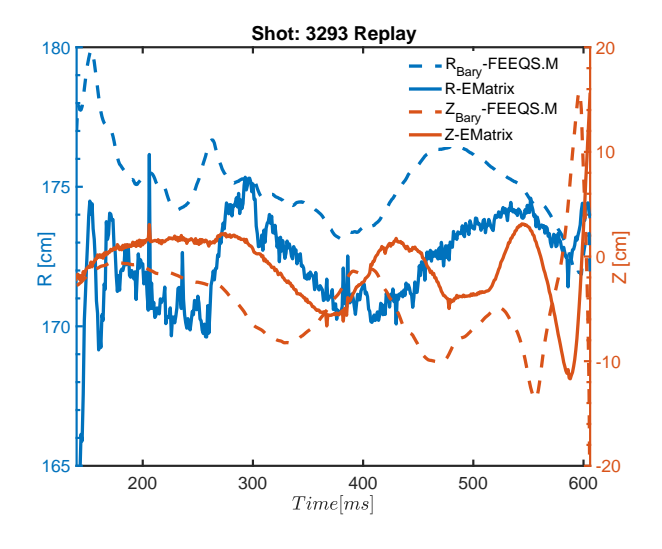


FIG. 4. Comparison of V_{PFs} between FEEQS.M simulation (dashed line) and experiment (plain line) for #3293.



 $FIG. 5.\ Plasma\ position,\ R\ and\ Z,\ estimated\ by\ FEEQS.M\ (dashed\ line)\ simulation\ and\ calculated\ by\ experimental\ measurements\ (plain\ one)\ for\ \#3293.$

3.3. Avoidance of VDE by Optimization

Based on the analysis of possible cause of the VDE in subsection 3.2, the VDE-induced disruption could be avoided through FF optimization. An instructive validation is to rerun #3293 with an increased R^{Ref} , i.e. $R^{Ref} + 5cm$, while keep all the other setting of the coupled workflow unchanged.

The results of optimized simulation are given in Fig. 6. It is clear to see that the optimized case remains stable and shows no indication of a VDE, even though the j_{ϕ} parameters are preserved. The simulation is terminated at 635ms, corresponding to the end of pulse #3293. The comparison of plasma boundary also shows good agreement between the FEEQS.M simulation and EFIT up to 550ms. Beyond this time, the simulation remains stable in Z as I_p continues ramping up and j_{ϕ} oscillates much more drastically.

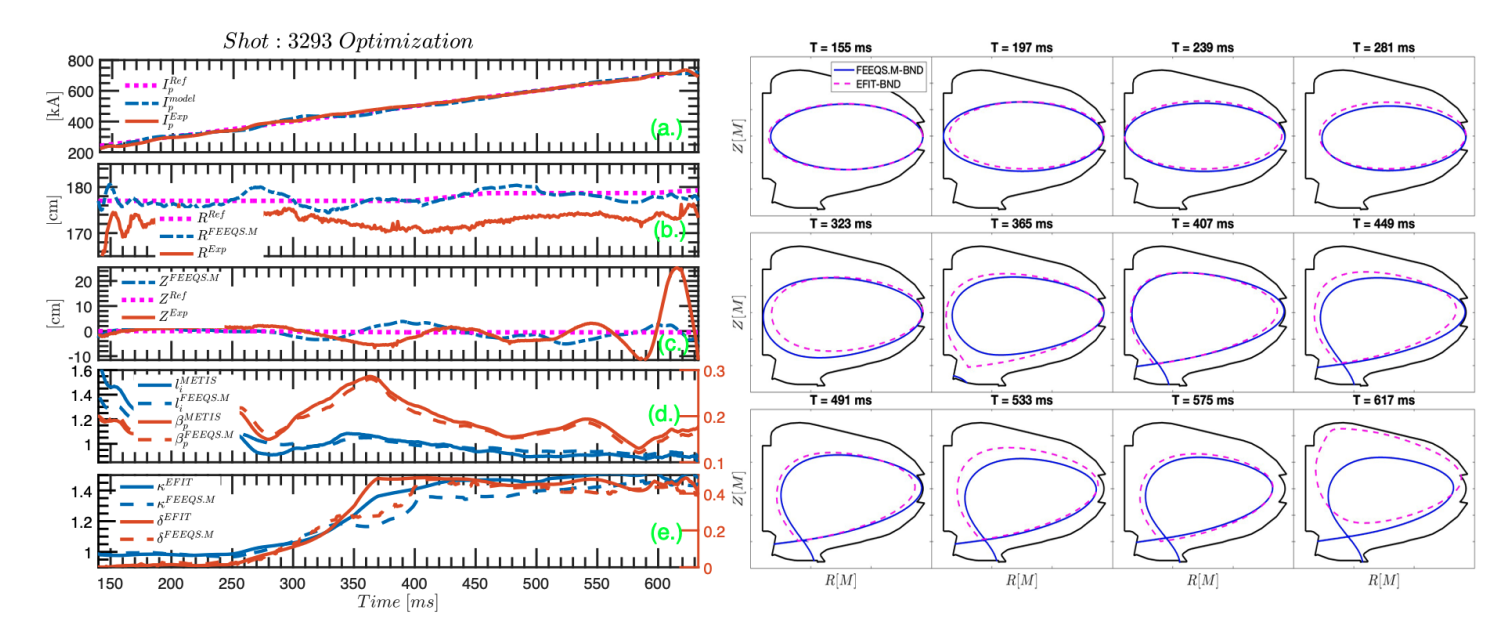


FIG. 6. Left: comparison between optimized simulation and experiment for #3293, (a) I_p , (b) R, (c) Z, (d) β_p and l_i , (e) κ and δ . Right: evolution of plasma boundary between magnetics-constrained EFIT and FEEQS.M.

The evolution of coil currents for the optimized simulation is shown in Fig. 7. It is found that at the beginning, when the plasma shape is in the limiter phase, all CS and PF coil currents closely match the experimental values, even though R^{Ref} has been increased by 5cm. After the onset of the limiter to divertor transition, starting at 250ms, the PF coil currents begin to deviate from the experimental values. Nevertheless, the VDE-induced disruption is successfully avoided in the optimized simulation, although coil currents in PF5 and PF6 are higher than those measured in experiment.

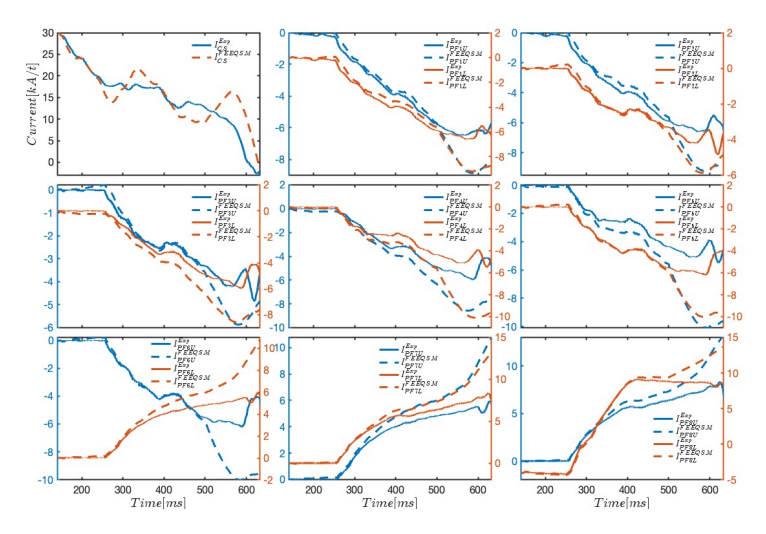


FIG. 7. Comparison of I_{PFs} between optimized FEEQS.M simulation (dashed line) and experiment (plain line) for #3293.

4. CONCLUSION AND FUTURE WORK

In this manuscript, a coupled workflow integrating the free-boundary equilibrium FEEQS.M and fast transport METIS codes, a simple I_p model and the plasma control strategy for target RZI_p has been developed to replay and optimize a VDE-induced disruption pulse in the HL-3 Tokamak. In FEEQS.M, plasma equilibrium and circuit equations are solved to obtain plasma boundary and position, coil currents and voltages. While in METIS, the magnetic diffusion equation is computed to get the plasma current profile. A simple I_p model, using inputs from FEEQS.M and METIS, is employed to link the two codes by providing a reliable evolution of I_p . The workflow is first validated by replaying pulse #3293, successfully capturing the experimental equilibrium, plasma boundary, and transport parameters. Analysis of the disruption indicates that underestimation of R is the primary contributor to trigger the VDE. By applying an optimized $R^{Ref} + 5cm$, the simulation achieved a stable limiter-to-divertor transition during the ramp-up phase, effectively avoiding the observed VDE-induced disruption. These results demonstrate the capability of the coupled workflow not only to reproduce experimental events accurately but also to provide actionable guidance for optimizing plasma control strategies.

For future work, the coupled workflow can be further enhanced in two key aspects. First, replacing the simple transport solvers in METIS with more robust source-and-sink libraries, particularly those accounting for various auxiliary heating and current drive mechanisms, would improve predictive accuracy and allow deeper physical insights into experimental scenarios. Second, incorporating surrogate modeling approaches, such as data-driven models or physics-informed neural networks, could accelerate computations by several orders of magnitude, enabling real-time or near-real-time predictive capability. Together, these improvements will establish the coupled workflow as a powerful tool for both experimental planning and predictive modeling, supporting the design of more reliable plasma scenarios and contributing to the broader development of disruption mitigation strategies in tokamak research, especially for the next generation of reactor-size plants.

ACKNOWLEDGEMENTS

This material is based upon work supported by the National Key R&D Project of China, under Awards 2019YFE03180004 and 2024YFE03180004.

REFERENCES

- [1] ZOHM, H., Philosophical Transactions of the Royal Society A 377 (2019) 20170437.
- [2] LAZARUS, E., LISTER, J., and NEILSON, G., Nucl. Fusion 30 (1990) 111.
- [3] SHAFRANOV, V., Sov. Phys. JETP 8 (1958) 494.
- [4] ANAND, H., WEHNER, W., ELDON, D., et al., Nucl. Fusion 64 (2024) 086051.
- [5] SONG, Y., ZOU, X., GONG, X., et al., Sci. Adv. 9 (2023) eabq5273.
- [6] OU, Y., XU, C., SCHUSTER, E., et al., Plasma Phys. Control. Fusion 50 (2008) 115001.
- [7] RAFIQ, T., KRITZ, A., WEILAND, J., PANKIN, A., and LUO, L., Phys. Plasmas 20 (2013).
- [8] HAWRYLUK, R., An empirical approach to tokamak transport, in Physics of plasmas close to thermonuclear conditions, pp. 19–46, Elsevier, 1981.
- [9] PEREVERZEV, G. V. and YUSHMANOV, P., ASTRA automated system for transport analysis in a Tokamak, IPP-Report 5/98 Max-Planck-Institut fur Plasmaphysik (2002).
- [10] CROTINGER, J. A., LLNL Report UCRL ID 126284, NTIS PB2005-102154 (1997).
- [11] ROMANELLI, M., CORRIGAN, G., PARAIL, V., et al., Plasma and Fusion research 9 (2014) 3403023.
- [12] KHAYRUTDINOV, R. and LUKASH, V., J. Comput. Phys. 109 (1993) 193.
- [13] WELANDER, A. S., WEHNER, W. P., PAJARES, A., and THOME, K. E., IEEE Trans. Plasma Sci. (2024).
- [14] ARTAUD, J.-F., IMBEAUX, F., GARCIA, J., et al., Nucl. Fusion 58 (2018) 105001.
- [15] GRAD, H. and RUBIN, H., Proceedings of the second united nations international conference on the peaceful uses of atomic energy, 1958.
- [16] HEUMANN, H., BLUM, J., BOULBE, C., et al., Journal. Plasma Physics 81 (2015) 905810301.
- [17] MOROSOHK, S., PAJARES, A., RAFIQ, T., and SCHUSTER, E., Nucl. Fusion 61 (2021) 106040.
- [18] SAUTER, O., ANGIONI, C., and LIN-LIU, Y., Phys. Plasmas 6 (1999) 2834.
- [19] SONG, X., LI, B., ZHOU, J., et al., Nucl. Fusion 61 (2021) 086010.
- [20] LAO, L. L., KRUGER, S., AKÇAY, C., et al., Plasma Phy. Control. Fusion 64 (2022) 074001.
- [21] ALBANESE, R., AMBROSINA, R., DE TOMMASI, G., et al., Nucl. Fusion 57 (2017) 086038.